PAPER

Transient non-classical transport in the hollow cathode plume I: measurements of time-varying electron collision frequency

IOP ebooks™

Bringing together innovative digital publishing with leading authors from the global scientific community.

Start exploring the collection−download the first chapter of every title for free.

Transient non-classical transport in the hollow cathode plume I: measurements of time-varying electron collision frequency

Marcel P Georgin[1,*] , **Benjamin A Jorns**[2] **and Alec D Gallimore**[2]

[1] University of Michigan, Applied Physics Program, Ann Arbor, Michigan 48109, United States of America
[2] University of Michigan, Department of Aerospace Engineering, Ann Arbor, Michigan 48109, United States of America

E-mail: georginm@umich.edu

Abstract
Electrostatic probes are employed to measure the time-variations in electron collision frequency due to a large-scale, low-frequency, plasma instability in a high-current hollow cathode plasma discharge (plume mode oscillation). Time-resolved measurements of ion acoustic turbulence are used to infer the effective collision frequency on the timescale of this underlying wave. Through a direct comparison, it is shown that the observed variation in the electron collision frequency cannot be described by classical collisional processes, i.e. Coulomb and neutral collisions, but rather is well represented by the changes in the anomalous collision frequency due to the turbulence.

Keywords: low-temperature plasma, plasma waves, plasma turbulence, hollow cathode, plasma propulsion, electric propulsion, ion acoustic turbulence

(Some figures may appear in colour only in the online journal)

1. Introduction

The hollow cathode is a low-temperature plasma electron source capable of producing a compact, dense, and current-carrying plasma. It is one of the most common and widely used forms of low-temperature plasma technology with applications that range from fundamental studies [1–5] to space propulsion [6] and materials processing [7, 8]. Despite over five decades of operational use, there remain aspects of the underlying physics in these devices that are poorly understood. For example, while under nominal conditions the plasma created by hollow cathodes is relatively stable, in certain circumstances these devices will transition to the so-called 'plume mode' and exhibit large scale (0.1–1 cm wavelengths), large amplitude (approaching 100% of time-average), low-frequency $\sim$100 kHz oscillations in plasma density and potential [9]. These fluctuations have been shown to adversely impact the power supply stability and cathode lifetime [10].

Given these deleterious effects, a number of best practices have been developed to avoid this unstable state. Nevertheless, the fundamental physical underpinnings of why the cathode transitions to plume mode remains one of the least understood processes in these devices.

The need to understand and ultimately avoid plume mode in hollow cathodes has motivated a number of studies into this phenomenon. Experimental advances over the past decade have led to several new insights into the nature of this mode. It has been shown, for example, that the onset of this oscillation can be linked to operating conditions where there is a high current to flow rate ratio [11–13]. Similarly, when the mode does appear at these conditions, the timescale of the oscillation is commensurate with the ionization rate downstream of the cathode exit in the near field plume [9]. Recently, high-speed imaging has confirmed that these plasma oscillations do in fact appear to originate at this location and propagate in both directions away from this point near the ion sound speed [14]. Significantly, although these empirical trends of

---

* Author to whom any correspondence should be addressed.

the plume mode have been established, capturing this transient effect self-consistently in numerical simulations has historically been a missing and critical capability [10] as modeling attempts have instead largely focused on the time-averaged plasma properties of the cathode plume.

With that said, there has been a recent breakthrough in the numerical modeling of the transition to plume mode. Simulations performed by two groups have been able to produce large-scale (0.1–1 cm) plasma oscillations [15–17]. The simulation results from Sary *et al* [16] have shown fluctuations that approached the amplitudes of those that have been reported experimentally (100% of the mean), though the dominant frequency of oscillation predicted, ∼1 MHz, was markedly faster than typical timescales of the plume mode (∼100 kHz) [9]. While the Sary model has yet to be validated against direct measurements from experiment, the modeling of Mikellides *et al* [17] has shown marked similarities in frequency and amplitude with direct experimental measurements of global plasma oscillations (keeper voltage) over a range of flow rates. The predicted plasma density oscillations produced by this simulation have exhibited qualitative and some quantitative similarities (such as frequency and propagation speed) to the time-resolved measurements of plasma density in reference [14]. Compellingly, this code also has shown the ability to re-create the experimentally-observed mode transition.

In both these recent modeling efforts, the ability to capture plume-mode like oscillations has been attributed to the inclusion of a model for non-classical electron collisions. The current-carrying plasma of hollow cathode plumes has been shown experimentally to support the onset of ion acoustic turbulence (IAT) [18–20]. The growth of these modes in turn is directly related to enhanced effective drag on the electrons. Previous modeling work has shown this non-classical effect must be included in numerical simulations in order to accurately represent the steep *time-averaged* gradients in plasma potential and electron temperature that are found in the cathode plume experimentally. The success of recent numerical works in exhibiting large scale oscillations suggests that this effective collision rate is also critically linked to the dynamical behavior of the plume mode.

Despite the compelling numerical results that point to the role of non-classical electron transport in the transition to plume mode in hollow cathodes, there is yet to be direct experimental confirmation that the wave-driven electron collision frequency varies on the timescale of the plume mode oscillations. Time-resolved probe measurements have indicated at least a correlational relationship with the presence of IAT [14]. However, it is not known if these fluctuations in turbulence drive the types of time-dependent, non-classical electron dynamics that have been incorporated in references [16, 17]. As an equally important practical consideration, even if the time-dependent anomalous collision frequency can be attributed to IAT, it is not clear how this should be modeled. The highest fidelity cathode models have been fluid-based; however, the onset of IAT and its contribution to the electron collision frequency is a kinetic phenomenon. In order to approximate the influence of the IAT on the plasmadynamics

in fluid models, it is necessary to adopt approximations, or 'closures', for the IAT's effect. Reference [17], for example, used a model based on the assumption the IAT was saturated [21] while references [15, 16, 20] employed a simplified quasilinear wave energy equation. While both of these models appear to approximate the time-average, non-classical electron dynamics well, it has not been shown experimentally if either model is actually valid on the timescale of the plume mode oscillation. This is a critical limitation as both studies concluded the non-classical transport is critical for driving the plume mode.

Given the purported critical role of the time-dependent non-classical electron collision frequency to the onset of plume mode, there is a pressing need for a detailed experimental investigation into this effect. In our previous work, we performed the initial step of showing experimentally that the IAT in a cathode plume does in fact vary on the timescale of the plume mode oscillation [14]. We expand upon this result of the previous study here with a two-part investigation. In the first part, we directly measure—for the first time—the effective electron collision frequency in the hollow cathode plasma on the timescale of the plume mode oscillation and compare it to contributions from classical and IAT-driven effects. In the second part (see [22]), we apply our experimental measurements to systematically evaluate different closure models adopted in fluid-based codes for the anomalous collision frequency.

With this in mind, this first part is organized in the following way. First, we introduce a theoretical framework to estimate the electron collision frequency from experimental data. We also include formulations for the expected collision frequency due to classical collisions as well as from the IAT. Following this, we describe the experimental apparatus and the *in situ* measurements used to extract both time-averaged and time-resolved plasma and IAT properties. We then present the results of the experiment and analyze the data to infer the plasma parameters. These properties are then combined to determine the total collision frequency. We compare our findings to the classical collision frequency and to the effective collision frequency determined from measured IAT spectra. Lastly, we discuss potential sources of uncertainty in our measurement.

2. Governing relations for the electron collision frequency

In this section we introduce a governing equation for inferring the electron collision frequency from experimental plasma measurements, and we review expressions for the contributions to this collision frequency from both classical and non-classical IAT-driven sources. For this discussion, we adopt the canonical geometry and coordinate convention shown in figure 1. The plasma discharge is axisymmetric connecting the electron source (the cathode) to a concentric anode mounted downstream. We assume the plume expansion is approximately conical as is qualitatively illustrated by the red dashed lines. In the following treatment, we consider expressions for the plasma properties as they evolve along the centerline of the discharge, exploiting the symmetries of the system.
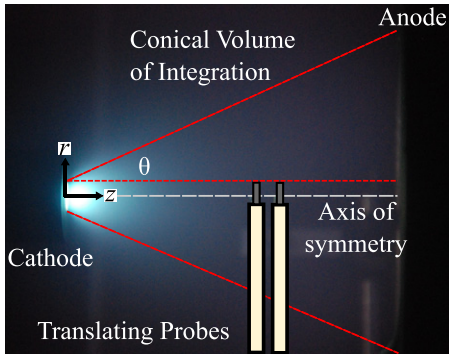
Figure 1. Experimental setup showing the cathode, anode, Langmuir probes, and coordinate convention. The origin $((r, z) = (0, 0))$ is located at the exit plane of the cathode and on cathode centerline. The operating condition is 20 A of discharge current and a flow rate of 5 sccm-Xe.

2.1. Direct estimate of collision frequency

Following reference [23], in our formulation for estimating the collision frequency we assume the cathode plume has negligible magnetic field and electron inertia can be neglected. This allows us to employ a generalized Ohm's law for the electron dynamics:

$$n_e m_e \nu_e \vec{u}_e = -q n_e \vec{E} - \nabla(n_e T_e), \quad (1)$$

where $\vec{u}_e$ denotes electron velocity, n_e is the electron density, ν_e is the electron collision frequency, q is fundamental charge, m_e is electron mass, $\vec{E}$ is the applied electric field, and T_e denotes electron temperature. In principle, (1) can be evaluated for the collision frequency everywhere in the plasma provided we make time-resolved measurements of the local electric field, electron drift, and plasma pressure. This would require, however, a full two-dimensional experimental map of the plume. To simplify the analysis and reduce the measurement domain, we instead only consider the electron dynamics along the discharge axis. Thus, (1) becomes one-dimensional, and we can invert to solve for the collision frequency:

$$\nu_e = \frac{1}{n_e m_e u_{e(z)}} \left(q n_e \frac{\partial \phi}{\partial z} - \frac{\partial (n_e T_e)}{\partial z} \right), \quad (2)$$

where z denotes the component along cathode centerline. Here we have used the electrostatic approximation to make the substitution $E_z = -\partial \phi / \partial z$ where ϕ denotes the local plasma potential.

Equation (1) provides a relation for electron collision frequency in terms of 1D measurements of the plasma parameters on centerline. While there are standard diagnostics to evaluate most of the key plasma properties, it historically has not been possible to measure the electron drift velocity directly with probes in hollow cathode plumes. In order to approximate this parameter, we invoke the electron continuity equation:

$$\frac{\partial n_e}{\partial t} + \nabla \cdot (n_e \vec{u}_e) = n_e \nu_{iz}, \quad (3)$$

where we have introduced $\nu_{iz} = n_n 10^{-20}(3.97 + 0.643 T_e - 0.0368 T_e^2)e^{-12.127/T_e} v_e$ [24] to represent the ionization collision frequency. In this expression, n_n and v_e denote the local neutral density and electron thermal speed, respectively. To relate (3) to $u_{e(z)}$, we make the assumption that the plasma undergoes a quasi-1D expansion from the cathode exit to the anode [25]. This allows us to write

$$u_{ez} = \frac{I_{dc}}{q n_e A} + \frac{\int (n_e \nu_{iz} - \frac{\partial n}{\partial t})A \, dz}{n_e A}. \quad (4)$$

Here we have introduced I_{dc} as the electron contribution to the discharge current (assumed to be approximately the same as the total value). The cross sectional area of the plasma is denoted as A. Earlier analyses of cathode plume measurements have shown that the time-average plasma density profile along centerline can be well described by assuming a conical expansion of the fluid [24, 26]. This approximation has been employed in previous work to extract the electron drift in this system to correctly predict the growth rate of IAT [19]. This simple model is also supported by electron streamlines in simulations [20] that show an angle of expansion $\sim 20°$–$45°$, though we note that our experimental configuration does not precisely match that of the simulation (cathode design and anode position). Given the experimental and numerical support for this approximation, we adopt it here and define the cross-sectional area $A(z) = \pi r^2(z) = \pi(r_o + \tan(\theta)z)^2$. In this expression, r is the radius describing the circular cross sectional area of the plume, r_o denotes the radius of the plume at the origin, and θ is the half-angle of conical expansion. Experimentally, r_o is known from the geometry, allowing us to curve fit plasma density measurements to estimate the divergence angle that we use to analyze the area in (4).

Applying these assumptions, (4) now depends on the centerline values of the plasma density, electron temperature, and neutral density. While we can measure the first two *in situ* with standard probing, we need to employ an additional approximation to estimate the neutral atom density. To this end, we model the evolution of the neutral density as a thermally expanding fluid from the cathode orifice, where the ionization of the gas primarily occurs inside the device with relatively few ionization events in the plume region. We therefore express the neutral continuity equation as $\partial (n_n u_n)/\partial z = 0$. This model in effect prescribes an upper bound for the neutral density in the plume by neglecting ionization losses in the neutral continuity equation. Employing this simplification avoids solving a partial differential equation for the density, which given the experimental uncertainty could lead to unphysical results. Further justification of this assumption and its implications are discussed further in section 5.1. Following the description above, we are physically treating the cathode orifice as a small point source from which neutral gas emanates. The neutral expands thermally, filling the available volume spherically from this point with $u_n \sim v_n = \sqrt{8/\pi k_B T_n/m_i}$, where k_B is the Boltzmann constant, and T_n is the neutral temperature. This physical picture for the neutral gas follows the 'ray-tracing' treatment of neutrals in the plume region of fluid codes [27]. Adopting

this description for the atoms, in our approach we allow the neutral gas to expand at a constant solid angle. Integrating the continuity equation, assuming constant velocity, we have:

$$n_{\mathrm{n}}(z) \simeq \frac{A_{\mathrm{n}}(0)}{A_{\mathrm{n}}(z)} n_{\mathrm{n}}(0) = \left(\frac{1}{\alpha_{\mathrm{iz}}(0)} - 1 \right) n(0) \frac{A_{\mathrm{n}}(0)}{A_{\mathrm{n}}(z)}, \quad (5)$$

where $A_{\mathrm{n}}(z)$ is the expansion area of the neutral gas and $\alpha_{\mathrm{iz}}(0)$ is the ionization fraction of the plasma at origin. Applying our assumption that the atom fluid expands at a constant solid angle gives the ratio $A_{\mathrm{n}}(0)/A_{\mathrm{n}}(z) = (r_{\mathrm{o}}/(r_{\mathrm{o}} + z))^2$. Therefore from our measurements only the ionization fraction remains unknown. However, we can estimate this value based on numerical simulations of similar cathodes [17] that suggest it lies between 10% and 50%. We account for this additional uncertainty by sampling this span of ionization fractions 400 times and calculating an average and standard deviation for the neutral density profile. We further discuss the influence of our approximations for the neutral density on our results in section 5.1.

In summary, (2) and (5) provide a closed set of relations for calculating directly the electron collision frequency in the plasma provided we can measure key plasma properties. We discuss the experimental techniques for detecting these properties in section 3.

2.2. Expressions for expected contributions to electron collision frequency

Provided we ultimately can measure the effective electron collision frequency in the cathode plume (see (2)), our goal is to determine what the major contributions are to this transport. To this end, we review here expressions for both classical and non-classical, IAT-driven collision frequencies. The classical expressions for electron–neutral and electron–ion collisions are given by ([24, 28]):

$$\nu_{\mathrm{ei}} = 2.9 \times 10^{-12} n_{\mathrm{e}} \frac{\ln \Lambda}{T_{\mathrm{e}}^{3/2}}$$

$$\nu_{\mathrm{en}} = 6.6 \times 10^{-19} \left(\frac{\frac{T_{\mathrm{e}}}{4} - 0.1}{1 + \left(\frac{T_{\mathrm{e}}}{4} \right)^{1.6}} \right) n_{\mathrm{n}} \sqrt{\frac{8T_{\mathrm{e}}}{\pi m_{\mathrm{e}}}}, \quad (6)$$

where Λ denotes the Coulomb logarithm. Non-classically, as discussed in section 1, the growth of IAT also can contribute to an effective collision frequency for the electrons. This stems from the fact that these waves are driven unstable by the presence of the high electron drift through the collisionless process of inverse Landau damping. Through a quasilinear formulation, the energy and properties of these waves can be related to an effective collision frequency (c.f references [21, 29]):

$$\nu_{\mathrm{an}}^{\mathrm{IAT}} = \frac{1}{n_{\mathrm{e}} m_{\mathrm{e}} u_{\mathrm{e}}} \sum_k \frac{k}{\omega_{\mathrm{r}}} W_k \gamma_{\mathrm{IAT}}^{\mathrm{e}}, \quad (7)$$

where k denotes the wavenumber in the direction of electron drift, W_k is the wave energy density of the kth mode in the IAT spectrum, ω_{r} is the frequency associated with the kth mode, and $\gamma_{\mathrm{IAT}}^{\mathrm{e}}$ is the electron contribution to the IAT growth rate due to inverse Landau damping. Physically, this expression shows

that as the energy in the waves and the rate at which the energy is extracted from the electrons increase, there will be a larger effective drag on the species. Following [18], we can simplify this expression by leveraging the properties of the ion acoustic modes in the IAT to find [19]

$$\nu_{\mathrm{an}}^{\mathrm{IAT}} = \sqrt{\frac{\pi}{2} \frac{m_{\mathrm{i}}}{m_{\mathrm{e}}}} \sum_{\omega_{\mathrm{r}}} \left(\frac{\tilde{\phi}_{\omega_{\mathrm{r}}}}{T_{\mathrm{e}0}} \right)^2 \omega_{\mathrm{r}}, \quad (8)$$

where $\tilde{\phi}_{\omega_{\mathrm{r}}}$ is the amplitude of the potential fluctuation with frequency ω_{r} and $T_{\mathrm{e}0}$ is the time-average electron temperature. These potential fluctuations can be related to the plasma density if we assume a collisionless, Boltzmann, probe sheath. In this scenario, $\nabla(n)/n = \nabla(\phi)/T_{\mathrm{e}}$, which under the assumption of constant electron temperature on the short time scale of the ion acoustic waves can be linearly perturbed to first order such that $\tilde{n}_{\mathrm{e}}/n_{\mathrm{e}0} = \tilde{\phi}/T_{\mathrm{e}0}$. Thus for each mode in the IAT spectrum with frequency ω_{r} we can express the anomalous collision frequency in terms of the electron density fluctuations, relative to the mean value:

$$\nu_{\mathrm{an}}^{\mathrm{IAT}} = \sqrt{\frac{\pi}{2} \frac{m_{\mathrm{i}}}{m_{\mathrm{e}}}} \sum_{\omega_{\mathrm{r}}} \left(\frac{n_{\mathrm{e}(\omega_{\mathrm{r}})}}{n_{\mathrm{e}0}} \right)^2 \omega_{\mathrm{r}}, \quad (9)$$

where $n_{\mathrm{e}(\omega_{\mathrm{r}})}$ is the amplitude of the density perturbation associated with the component of the IAT spectrum oscillating at frequency ω_{r}, and $n_{\mathrm{e}0}$ represents the time average electron density. Armed with this result, provided we can measure the power spectrum of the IAT relative density fluctuations on the timescale of the plume mode, we can infer the effective non-classical, wave-driven collision frequency.

3. Experimental setup

In this section, we describe the experimental setup to measure the plasma properties necessary to evaluate the overall effective collision frequency (see (2)) and the contributions to this collision frequency (6) from classical and non-classical effects (7). We describe our technique for achieving the necessary time resolution to observe variations of these key plasma parameters on the timescale of the plume mode oscillation.

3.1. Cathode and probes

The test article we employed for this investigation consisted of a 20 A class LaB$_6$ hollow cathode with a 3 mm tungsten orifice and a graphite keeper at a flow rate of 5 sccm of xenon gas [30]. The plasma discharge was maintained at 20 A of discharge current to a cylindrical, water-cooled anode positioned 45 mm downstream of the keeper exit. No external magnetic field was applied. The cathode was fired in a 0.5 m × 1 m vacuum chamber that achieved a base pressure of 0.1 μTorr and an operating pressure of 20 μTorr-Xe through cryogenic pumping.

Figure 1 shows a sideview of the experimental setup for this work along with a notional schematic of probe location. We used three types of probes to characterize the key properties: an emissive probe, a floating probe, and an ion saturation current probe. The emissive probe consisted of a loop of

thoriated-tungsten wire. The floating and ion saturation probes were identical, with dimensions of 2 mm long and 0.12 mm in diameter. Each probe was capable of translating along the axis of symmetry of the cathode from the keeper surface ($z = 0$ cm) to the anode. The measurements from each probe in turn were sampled at a rate of 10 MHz, well in excess of the plume mode characteristic frequency. For the results reported in this work, we measured from 0.1 cm to 0.9 cm from the cathode with a spatial resolution of 0.1 cm. The frequency resolution was 10 Hz.

3.2. Probe analysis technique

We discuss in the following the analysis techniques we employ to convert time-resolved data from the probes to measurements of the spatially and temporally resolved properties of the plasma along cathode centerline. We can relate the emissive probe floating potential, V_{em}, to the plasma potential, Φ, and electron temperature, T_e, through

$$V_{em} = \Phi - T_e. \tag{10}$$

The temperature correction employed in this expression accounts for space-charge effects [31]. This relation requires a measurement of the electron temperature, which we can determine following [32] as

$$T_e = \frac{2(\Phi - V_f)}{\ln\left(\frac{2}{\pi}\frac{m_i}{m_e}\right)}, \tag{11}$$

where V_f is the floating potential. Combined, this set of equations allows us to self-consistently solve for both the electron temperature and plasma potential from the measured emissive probe voltage and the floating voltage.

For the electric field, we take the plasma potential and calculate the spatial gradient, $E = -\partial\Phi/\partial z$. For the plasma density, we analyze the ion saturation current under the thin sheath and quasi-neutrality approximations. The former assumption previously has been explored and shown to be valid for the hollow cathode plasma where the Debye length of these plasmas is typically between $1-10$ μm, orders of magnitude smaller than the probe radius [9, 14, 19]. As such we calculate the density as

$$n_e = \frac{I_{sat}}{0.61 A_p c_s}, \tag{12}$$

where I_{sat} is the ion saturation current, $c_s = \sqrt{qT_e/m_i}$ is the Bohm speed, and A_p is the probe area.

Finally, in order to evaluate the contributions from wave energy to IAT with (7), we follow the approach outlined in references [14, 18, 19] by summing over a Fourier decomposition of the relative density fluctuations. To estimate this ratio, we make the assumption $\tilde{n}_e/n_{e0} = \tilde{I}_{sat}/I_{sat0}$, where the tilde indicates the fluctuations and the subscript 0 is the time-average value. This equivalence is valid provided the sheath at the probe adjusts to the wave potentials faster than the timescale of oscillation and that the temperature fluctuations on the timescale of the acoustic modes are negligible. As the characteristic timescale for sheath adjustment is on the order

of the ion plasma frequency and the measured IAT spectra typically is an order of magnitude lower than this frequency, the first assumption is satisfied. Similarly, the ion acoustic dispersion is contingent on the assumption of isothermal electrons on the timescale of oscillation. Since the IAT dispersion has been measured and validated against experiment extensively in previous work [14, 19, 33, 34], the assumption of low temperature fluctuations on this timescale also is appropriate. With that said, we did not have the ability to directly verify the assumptions that allow us to equate fluctuations in density and ion saturation. This caveat should be borne in mind in the following discussion.

3.3. Time synchronization

The evaluation of (2)–(7) requires spatially-resolved measurements of the plasma properties on the timescale of the plume mode oscillation ($\sim$100 kHz). To this end, we adopted the triggered average approach based on the method outlined in [14]. This technique is contingent on the plasma properties exhibiting at a relatively coherent oscillation (as we anticipate for plume mode). We first recorded the time-history of the ion saturation probe at each spatial location. We simultaneously measured the time-history of the discharge current. This process is repeated for the floating and emissive probes. In order to sync these disparate measurements in time, we used the periodic peaks in the discharge current signal (passed through a bandpass filter) as a consistent reference in phase. We then averaged over 5000 cycles to reduce the signal-to-noise ratio. This yielded waveforms for each plasma parameter as a function of phase offset with respect to the discharge current peak. We note that we explicitly assume that the oscillations were consistent in phase rather than in time. This phase averaging, rather than time averaging of the waveform, produced more consistent results as the frequency of the plume mode oscillation tends to drift in time. The advantages of phase referencing were noted in previous work where similar techniques were successfully employed for time-resolved measurements of plasma properties in a Hall thruster [35].

While the plasma property measurements yielded by the triggered averaged technique allow us to estimate the effective collision frequency and contributions from classical effects, the time-resolved estimate of the anomalous collision frequency from IAT requires a more nuanced treatment. Implicit in our approach (and as was discussed in our previous work [14]) is that the constituent ion acoustic modes in the IAT oscillate on a much shorter timescale than the low-frequency plume mode oscillations. With this in mind, we use the same triggering scheme as described above where we subdivide the original time-resolved measurements of ion saturation current into single cycles based on peaks in the discharge current oscillation. We then subdivide these current traces into seven segments and divide each segment by the time-averaged mean. This yields seven bins with time-resolved measurements of the relative fluctuations in ion saturation current (and by proxy, density), $\tilde{n}_e/n_{e(0)}$. We then calculate the power spectrum for each segment and perform a frequency-weighted summation to determine the contributions to the collision frequency from

the IAT (see (7)). The end result is a set of seven bins equally spaced in phase with the magnitude indicating the variation in ν_{an}^{IAT}

4. Results

In this section we present the results of our experiment and preliminary analysis. We first discuss the time-average measurements of the plasma parameters and collision frequency. We then show the time-resolved calculation of the classical, non-classical, and total electron collision frequencies.

4.1. Time-averaged measurements

Figure 2 shows the probe measurements and the plasma parameters inferred from these measurements as a function of distance from the cathode. The first, figure 2(a), illustrates the emissive probe and floating probe voltage. We note that there is a discontinuity in the emissive probe voltage that is likely the result of probe perturbations, the effect of which we discuss in section 5.1. The solid curve is a cubic spline fit to the emissive probe voltage to smooth the spatially resolved profile. The second plot, figure 2(b), shows the time-averaged plasma potential, floating potential, electric field, and electron temperature calculated from the smoothed trace of the emissive probe measurement and (10) and (11). The third plot, figure 2(c), shows the electron density, calculated from (12), and the Mach number, $M_e = u_e/\sqrt{qT_e/m_e}$, as a function of position.

The uncertainty of the parameters shown in figure 2 stems from the standard error in the time-resolved emissive and floating probe measurements. We propagated these errors forward into the calculation of the plasma properties in figure 2(b) through (10) and (11). The error in the plasma density is $\sim 15\%$, which primarily stems from our uncertainty in the probe dimensions. The error in the electron Mach number is dominated by the uncertainty in the half-angle of expansion, affecting the cross-sectional area $A(z)$ in (4) and (5). Here we calculated the uncertainty by curve fitting the plasma densities at each time point during the plume mode oscillation to determine the expansion area 50 times. We then take the standard deviation of this data set as the uncertainty and propagate it through to electron Mach number.

As is characteristic of the cathode discharge, the plasma density shown by figure 2(c) is monotonically decreasing with distance from the cathode. Physically, this decrease is indicative of the conical expansion of the plume and results in an order of magnitude reduction over the measurement domain. The expansion angle found from our curve fit is $\theta = 24° \pm 2.6°$, which makes physical sense as this value is less than angle subtended by the anode $(30°)$. The plasma potential follows an opposite trend compared to the plasma density, showing a rise from the cathode to anode. This suggests that the electron dynamics are not governed by the Boltzmann relation but rather there are other driving factors. Indeed, this trend is consistent with previous work [9] where it has been shown that the plasma potential increase is indicative of the presence of IAT and the associated non-classical resistance [23]. The strong in the electric field (as inferred from the plasma potential measurement) near the cathode is necessary to drive current through this non-classical resistance. The electric field in turn promotes non-classical Ohmic electron heating as can
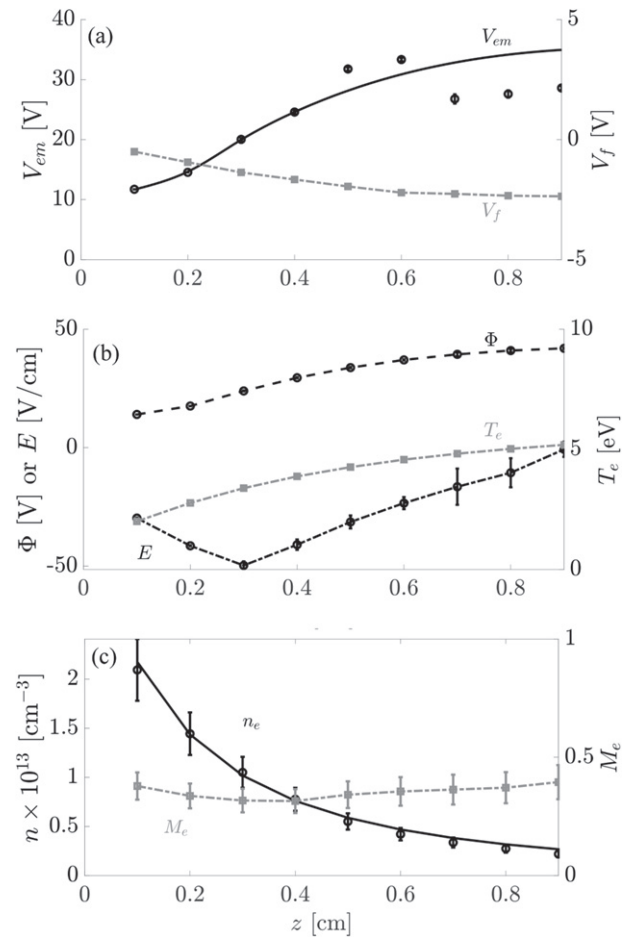

Figure 2. Time-average probe measurements along centerline in the plume of the hollow cathode as a function of distance from the cathode keeper $(z = 0 \text{ cm})$. (a) is the emissive probe voltage, and floating voltage. The solid line is a spline fit to the emissive probe voltage. (b) is the plasma potential, temperature, and electric field. (c) is the electron density and Mach number. The solid line is a curve fit to the data assuming a conical expansion of the plasma. The expansion angle determined from the fit is $24° \pm 2.6°$.

be seen by the rise in temperature from 2 eV near the cathode to 5 eV downstream. This increase occurs despite the fact that the plasma is expanding (which would lead to classical cooling). As shown in figure 2(c), the electron Mach number is approximately constant as a function of position. This is consistent with the findings of previous work [19] and is the result of a combination of two effects. The density decreases as the plasma expands away from the cathode, the electron drift velocity increases. This is balanced by the increase in the thermal velocity that results from the heating of the electrons with position.

We show in figure 3 the Fourier transform of the relative fluctuations of the ion saturation current at three axial distances from the cathode exit. These results are qualitatively consistent with the data presented in previous work [14, 18, 19] and exhibit two distinct types of oscillations. The first is the plume mode which is characterized by the large amplitude oscillation at $f = 40$ kHz with its associated harmonics. The second class of oscillations exhibits high-frequency, broadband waves between ~ 100 and 1000 kHz. This spectral
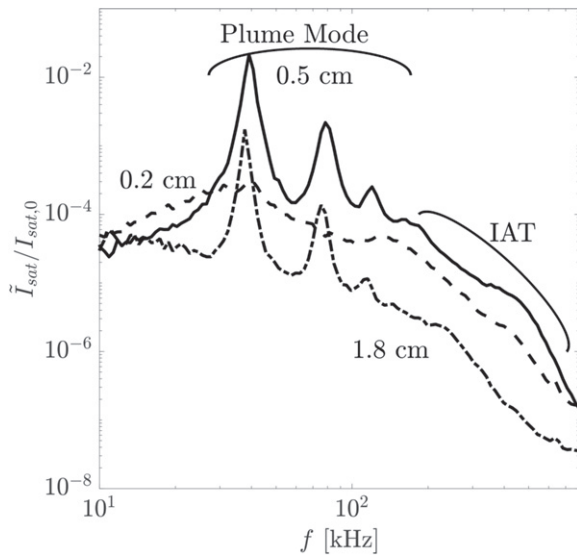
Figure 3. Fourier transform of the relative fluctuations in ion saturation at different distances from cathode. The plot is smoothed by logarithmic binning of the data.

Figure 4. Steady-state collision frequencies along cathode centerline as a function of distance from cathode exit. The gray bands indicate the uncertainty.

content is indicative of IAT. As shown in figure 3, we see that at positions nearest the cathode, the characteristic peaks of the plume mode oscillation are not observed in the power spectrum. Further downstream at $z = 0.5$ cm, these large amplitude modes appear and decrease in amplitude with increasing distance. Similarly, the amplitude of the higher frequency IAT modes rises between 0.2 cm and 0.5 cm and then decreases as a function of position.

We now use our results to compute the electron collision frequency in the plume and estimate the contributions from classical and non-classical effects. To this end, we used the data from figure 2 to calculate the total electron collision frequency with (2). We show this result as ν_e in figure 4 where the effective collision frequency is on the order of GHz. This result is consistent with previous experimental [18] and numerical findings [10, 23].

In order to evaluate what could be driving this measured collision rate, we use the plasma properties in figure (2) to estimate the classical components from (6) and the IAT amplitudes from figure 3 to infer the anomalous electron collision frequency with (7). For this latter collision frequency, we have only summed over contributions from the spectrum above 300 kHz to separate the high-frequency turbulence from the low-frequency plume mode oscillations. Figure 4 shows all these frequencies as a function of position in the cathode plume. The gray bands represent the uncertainty in each calculated frequency, which we estimated by propagating error in the plasma parameters through the respective governing equation. As figure 4 shows, the classical collision frequency is orders of magnitude lower than the measured rate. This confirms that the collision frequency is in fact non-classical in the plume. Moreover, the anomalous collision frequency inferred from quasilinear theory can explain the measured collision frequency (within statistical uncertainty) over the majority of the plume, i.e. between positions 0.3 cm and 0.9 cm. We do note
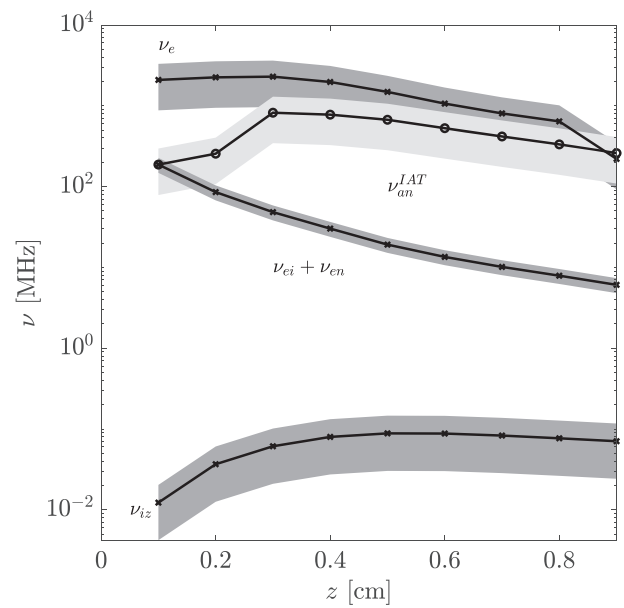
that there is disagreement between the anomalous collision frequency and the measured electron collision frequency at the two points nearest to the cathode. The physical explanation for this discrepancy is not immediately evident. It is possible that there may be another mechanism driving the collision frequency at this location aside from IAT. However, we also note that this location is where we started to see marked perturbation of the plasma introduced by the insertion of the probe. The result therefore may not be physical (section 5.1). With that caveat in mind, we in general find that in the plume region the magnitude and trends in the electron collision frequency can be accurately predicted from wave measurements and quasilinear theory. This result is consistent with previous findings, [18, 19, 23], though we note this is the first spatially-resolved experimental comparison of the measured effective collision frequency in the cathode plume to the IAT-driven anomalous collision frequency inferred directly from measurements of wave properties.

4.2. Time-resolved measurements

Now that we have shown that the effective collision frequency due to the IAT can explain the electron transport in the plume, we try to determine if this relationship holds on the timescale of the plume mode oscillation. Our earlier work in [14] offered some insight into this question, showing correlationally that the amplitude of the IAT is fluctuating on the timescale of the plume mode. However, we did not have the ability in this previous work to relate these measurements directly to an IAT-driven collision frequency, and we did not have direct measurements of the electron collision frequency for comparison. To expand on these previous findings, in this section we follow the general approach outlined in section 4.1 to estimate the electron collision frequency and contributions from classical and non-classical effects. The time-resolved measurements were
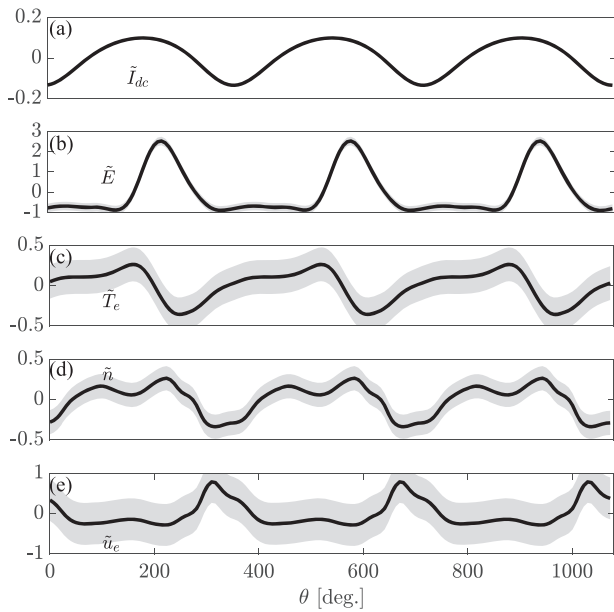
Figure 5. Relative fluctuations of the (a) discharge current, (b) electric field, (c) electron temperature, (d) plasma density, and (e) electron velocity at $z = 0.5$ cm. The gray area represents the standard deviation.

Figure 6. Comparison of the measured electron collision frequency to the anomalous (7) and classical (6) collision frequencies at $z = 0.5$ cm. The gray area represents the standard deviations.

generated following the triggered average procedure outlined in section 3.3.

Figure 5 shows the relative fluctuations in the plasma parameters calculated from (11) and (12) at a location $z = 0.5$ cm and plotted as a function of phase angle with respect to the discharge current. In all cases, we have subtracted out the mean and normalized the fluctuations to the local mean value, e.g. $\tilde{n} = (n - \bar{n})/\bar{n}$, where $\bar{n}$ indicates the time average value. We highlight this particular location because this is where we observed the highest fluctuations in electron temperature in the spatial domain. In descending order, we show the discharge current, electric field, electron temperature, plasma density, and electron drift velocity. The estimated uncertainties are indicated by the gray bands. The error in the density, temperature, and electric field is derived from standard deviation of the raw time-resolved probe measurements and is typically 20% of the time-average value, i.e. 0.2 on the plots. Propagating these uncertainties, along with the uncertainty in the plasma area, through (4), we find that the error in the electron drift velocity is ~50% at this location.

The discharge current oscillation shown in figure 5(a) has a peak-to-peak value of ~20% on average but instantaneously can be 40% the average value. As reported in reference [9], this degree of variation is typical of a hollow cathode discharge when operating in plume mode. In figure 5(b), we see the relative amplitude of the electric field fluctuation exhibits the highest variation of all the measured plasma properties, peaking at ~2.5 times its mean value. The field similarly exhibits a peak that is approximately in phase with the peak in discharge current. Physically, this is an intuitive relationship that reflects the fact that as the electric field increases, more electrons are
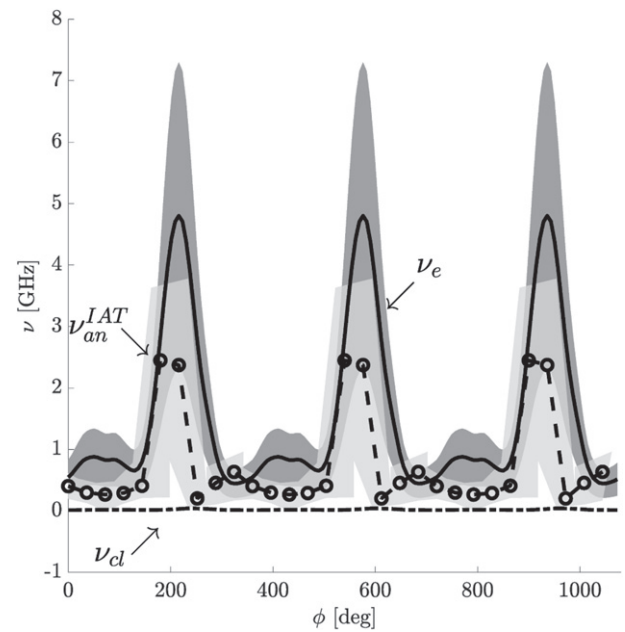
pulled towards the anode, thereby increasing the discharge current. Figures 5(c) and (d) show the electron temperature and plasma density, respectively. We see here that the oscillations in these parameters have similar cnoidal structure in time, which is reflected in the harmonics exhibited by the power-spectra of the ion saturation current in figure 3. The complex phase and amplitude relationships between these properties are nuanced, underscoring the interdependence of heating, convection, and ionization in the plume region. Lastly, we show the electron drift velocity in figure 5(e) that we evaluated from (4). In this case, we see that the variations in this parameter are ~180° out of phase with the plasma density. This relationship broadly can be understood from conservation of current. Though, we note that the phase offset is not perfectly anti-correlated. Small in-phase components in density and velocity produce the oscillations in discharge current.

4.3. Measurement of the anomalous collision frequency

Synthesizing the results above, we use our measurements of the time-dependent plasma parameters in figure 5 to calculate the collision frequency in the plume by evaluating the 1D Ohm's law in (2). In figure 6, we compare this measured value to the estimates of the classical (6) and non-classical contributions [using the time-syncing technique and (7)] to the electron collision frequency. In this plot, the gray shaded areas represent the uncertainty in ν_e (dark gray) and ν_{an}^{IAT} (light gray). For ν_e, the error is determined by propagation of the uncertainty in the parameters in figure 5 through (2). For the IAT contribution, the uncertainty is calculated from the standard deviation of the 5000 cycles used in the time-syncing and averaging process detailed in section 3.3. Figure 6 shows that the electron collision frequency exhibits a marked oscillation with cnoidal structure at this location. The amplitude is large,
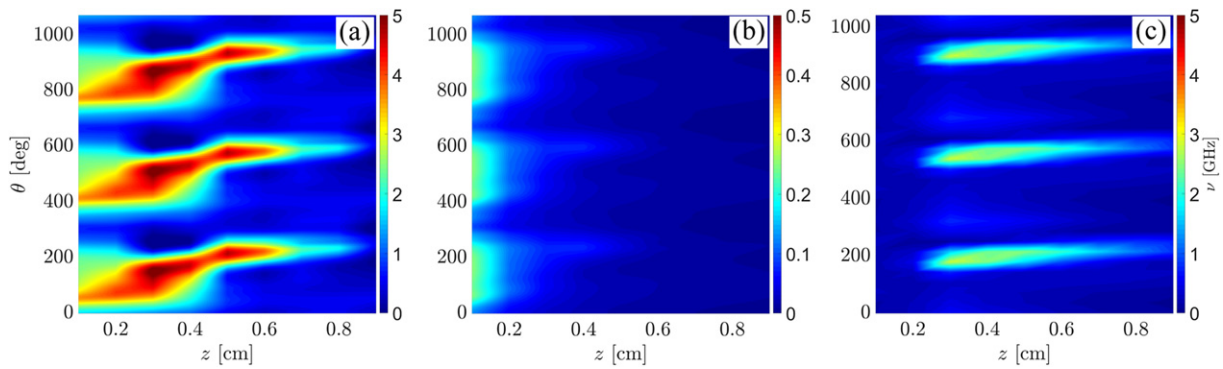
8

Figure 7. Comparison of the collision frequencies as a function of position and time. (a) is the measured collision frequency. (b) is the classical contribution. (c) is the anomalous component. Note the change of scale in (b) to show the oscillation detail.

approximately 100% the mean value. Comparing figures 5 and 6, we find that the collision frequency is in phase with the electric field. From a physics standpoint, this finding indicates that when the electron collision frequency rises, the plasma responds with an enhanced electric field to pull those electrons to the anode.

Figure 6 shows the comparison between the measured electron collision frequency and the values based on the classical and non-classical equations presented in section 2.2 at $z = 0.5$ cm. Comparing to the time-averaged results (figure 4), we find comparable relationships in the relative magnitudes. The classical collision frequency is several orders of magnitude smaller than the measured collision frequency while the time variations of the wave-driven collision frequency are on the same scale as the electron collision frequency. Indeed, the anomalous collision frequency is within statistical uncertainty of the measured values, exhibiting high correlation in both magnitude and time. Ultimately, this is a major new contribution from this study as figure 5 shows, for the first time, that the time variations in the electron collision frequency on the timescale of the plume mode oscillation are indeed driven by changes in the anomalous collision frequency from IAT.

Expanding upon our single point measurements above, we next explore the trends over the whole measurement domain in figure 7. Figure 7(a) shows the measured collision frequency as a function of space and time. The oscillation amplitude increases from 0.1 cm to 0.4 cm and decreases towards the anode. Qualitatively, this result parallels the findings of high-speed camera measurements in [14], which indicated that oscillations in plasma luminosity reached a peak at a location downstream of the cathode and decayed in amplitude from this position both towards the cathode and the anode. Further corroborating the earlier results, figure 7 shows that the oscillation in collision frequency propagates near the ion sound speed at 3 km s^{-1} on average over the length structure. This value, however, can be as low as 1 km s^{-1} at $z = 0.4$ cm or as high as 6 km s^{-1} at $z = 0.6$ cm.

For our first comparison, we plot in figure 7(b) the spatially and temporally resolved classical collision frequency. Noting the scale, we find that the classical collision frequency quantitatively underestimates the measurement in figure 7(a) by more than an order of magnitude over the experimental domain.

However, we remark that the waveform of the classical collision frequency at least exhibits qualitative similarities to the measured value in the near-field region ($z < 0.2$ cm). Now turning to figure 7(c) where we plot the anomalous collision frequency on the same scale as the measurement in figure 7(a). In the region beyond $z = 0.2$ cm, we find both quantitative and qualitative agreement in the spatio-temporal evolution of this oscillation with the measured collision frequency. In this part of the domain, the oscillation amplitude is predicted to within a factor of two, which is within the uncertainty of the measurement. However, this agreement disappears in the near-field region ($z < 0.2$ cm), where the estimated anomalous collision frequency is much lower. In our earlier time-averaged results (see figure 4), we identified a similar disagreement in this region and proposed that this could be because of probe perturbations affecting the IAT amplitude.

Physically, figure 7 indicates that for most of the cathode plume (beyond the very near-field region), the effective drag force generated by the IAT is enhancing the resistance of the plasma. Further, time-variations in the IAT amplitude dictate the evolution of the overall plasma resistance. These changes in resistance, in turn, cause the characteristic discharge current oscillations of the plume mode. The fact that the anomalous collision frequency does vary as a function of time is thus a corroboration of the hypothesis proposed to date in the numerical models of the plume mode oscillation [15–17].

5. Discussion

The results presented above illustrate the critical importance of the IAT driven-collision frequency for capturing the time-average and time-resolved properties of the hollow cathode plume. In this section, we first detail potential caveats and sources of systematic uncertainty in our analysis. We then discuss the physical implications of this result for the understanding of modeling of hollow cathode plumes [15, 20, 23].

5.1. Sources of systematic uncertainty

As we have discussed in earlier sections, the uncertainty attributed to our results stems from the statistical variations in our measurements; however, there also exist sources of systematic error that can influence our findings. These systematic

uncertainties primarily originate from our experimental apparatus and the probe analysis techniques and assumptions used infer the plasma parameters. In this section, we discuss the possible influence of these two inherent error sources on our findings.

5.1.1. Role of probe perturbations.

As we briefly noted in section 4, our probing methods likely introduced perturbations to the local plasma properties. Indeed, the perturbative effect of electrostatic probes remains an active area of research in plasmas for electric propulsion [36, 37] where it has been found that the presence of these conducting structures can cause changes to the local and global plasma properties. Most notably, in our axial sweeps, we found that the discharge voltage would change by 1–2 V as the probes moved closer to the cathode. In the case of the emissive probe, this was accompanied by a noticeable discontinuity in the measurement between 0.6 cm and 0.7 cm in figure 2(a). This discontinuity was not observed in the other probes, and we believe it is the result of perturbation effects. The physical reasoning for this is that we do not expect this type of stark reversal of the electric field as indicated by the unprocessed data. If this were a real effect, then the Ohm's law in equation (2) would suggest a reversal of the electron drift towards this 'local anode'. Consequentially, the neutral gas downstream of this region would have to be ionized to maintain current continuity to the anode. Noting the relatively low and decreasing ionization rate in figure 4 it appears physically implausible in our plasma. To address this non-physical result, ideally, we would have an independent, non-invasive metric for checking the plasma measurements as was done for Hall thruster studies in references [36, 37]. However, the key parameters of interest to us are the electron properties, and to date, with the exception of preliminary studies [38], there are no methods available for hollow cathodes for performing non-invasive characterization of these properties. As an approximation then, in section 4, we implemented spline smoothing to reflect our physical intuition that the discontinuous in potential was not physical. Generally, the use of the smoothed curve tends to reduce the gradients, leading to a reduction in the magnitude of the electric field and by Ohm's law the collision frequency.

In addition to affecting steady state plasma properties, the sharp discontinuity in the calculated anomalous collision frequency between 0.2 cm and 0.3 cm (see figure 4) indicates that the presence of the probe could be affecting the amplitude of the IAT propagating in the plume. In previous work [39], it has been noted that the use of electrostatic probes (approximately 10% the size of the plasmas) influences the amplitude of drift waves. Similarly, at these near-field locations, the cross sectional area of our probe approaches 10% of the estimated discharge area. Extrapolating from these earlier findings in [39], the likelihood that the probe disrupts the propagation of IAT increases as we approach the cathode in our spatial sweeps. Given that we find quantitative agreement (within statistical uncertainty) beyond $z = 0.3$ cm in figure 4, we suspect that the probe perturbation of the waves is smaller in this downstream region where the plasma has expanded. With that said, the fact that the probes could be perturbative to the plasma should be borne in mind as a significant caveat to our findings.

5.1.2. Validity of key assumptions in data analysis.

The limitations of our experimental capabilities and accessibility for this study required a number of assumptions in the analysis to infer the electron collision frequency. Although these approximations ultimately allow us to make comparisons between measurement and theory, they may be sources of additional uncertainty in our results. In this section, we discuss the degree to which these assumptions could influence our interpretation of the results.

We first remark on the assumptions inherent to the analysis of the raw probe data. The relations we have employed to analyze our measurements rely on the probe theory for a non-drifting, Maxwellian plasma. In contrast, our results suggest that the cathode plasma has a significant drifting component (see figure 2(c) and reference [40]). This drifting component can lead to changes in the estimates for the plasma density and temperature. To evaluate this effect, following Sheridan *et al* [41], we note that for an electron Mach number ∼0.3, the standard probe analysis method will overestimate the electron temperature by ∼10%. This overestimate in the temperature would translate in turn to an underestimate of the plasma density. Both effects would propagate through the continuity equation (4) and Ohm's law (see (2)), leading to an underestimated electron collision frequency by 10%. With that said, the uncertainties in these plasma parameters (Mach number, temperature and density) stemming from the probe analysis are within the reported measurement uncertainty. We thus do not expect the qualitative trends in the data to change nor will this systematic effect translate to quantitative changes in the results outside the reported confidence intervals.

Next we comment on our assumption of the quasi-1D expansion of the neutral gas. In implementing this approximation, we have calculated an upper bound on the effects of the neutrals on the plasma—notably the ionization rate and electron-neutral collision frequency—by neglecting ionization losses in the neutral continuity equation. Using the results from section 4, we can justify this assumption by comparing our upper bound estimate for the ionization rate in the plume to the expected influx of neutrals. Since ionization is a loss mechanism for this species, the criterion to neglect this term is

$$\frac{\frac{\partial n_{\mathrm{n}}}{\partial z} v_{\mathrm{n}}}{n \nu_{\mathrm{ion}}} \sim \frac{v_{\mathrm{n}}/L_{\mathrm{n}}}{n k_{\mathrm{ion}}} \gg 1, \tag{13}$$

where k_{ion} is the ionization rate coefficient and $L_{\mathrm{n}} \equiv \nabla n_{\mathrm{n}}/n_{\mathrm{n}}$ is the neutral density gradient lengthscale. Evaluating this criterion with our experimental measurements and inferred neutral density profile, we find that this non-dimensional parameter is ∼5–50 throughout the plume. This introduces an error of <20%, which when propagated to the collision frequency is already within the stated uncertainty.

Additional uncertainty on the neutral density calculation is introduced by assuming it is constant in time. Ionization is the primary process by which this density is modulated and the ratio we have calculated in (13) indicates that any depression in the neutrals density by ionization will quickly filled

by the influx of gas from the cathode. We also can derive an additional criterion for the relative importance of ionization on the variations in the neutral gas by examining the neutral continuity equation, neglecting the spatial derivative. Taking $(\partial n_\mathrm{n}/\partial t)/n_\mathrm{n} \sim \omega$, this analysis gives the ratio $\omega/nk_\mathrm{ion} \gg 1$ for neglecting ionization effects on the neutral density on the plume mode timescale. Experimentally, we find that this ratio to be between 10–100, which supports our assumption that fluctuations in the neutral density due to ionization are not likely significant at our operating condition. With that said, as the oscillations become larger at other conditions, the temperature and plasma density oscillations will modulate the neutral atom density further. While this mechanism does not inherently impact our conclusions about the effective collision frequency of the cathode plume, these atom density oscillations could still play an important role in the underlying mechanism for the plume mode.

As a final note on the neutral density, our results can provide additional post-hoc evidence to support this assumption that the neutral density fluctuations can be neglected in our analysis of the collision frequency. Specifically, we have found that the electron–neutral and ionization collision frequencies are orders of magnitude lower than both the measured total collision frequency and the contribution from IAT. This would suggest that even if we did allow for neutral density variations, these would not impact our conclusions about the time-resolved collision frequency and its relationship to the non-classical collision frequency resulting from the IAT.

Another key assumption we employed to reduce the complexity of our analysis was that we could treat the plasma expansion as quasi-one dimensional. Inherently, this formulation of the fluid equations implies constant density and electron velocity as functions of radial position and further signifies that the electron motion is purely in the axial direction. In section 2.1 we justified this assumption by noting that electron streamlines determined from numerical simulations indicate a primarily axial drift near the axis of the plume [20]. In practice, however, there are small but finite radial components to the electron drift. Our estimates for the axial electron velocity through our quasi-1D analysis thus is an upper bound and likely overestimate of the actual electron axial drift. As an example of how this could change our results, in the extreme case that the electrons are drifting at a 30° angle from the discharge axis (the angle subtended from the origin to the anode surface), we would have overestimated the electron drift by ~15%. This error is within the stated uncertainty of the electron drift. Therefore, we do not expect that this overestimate will change the qualitative trends in the data nor will it translate to quantitative differences in the results beyond the uncertainty in the measurement of the collision frequency.

As a final note, we revisit the expressions for the non-classical collision frequency presented in section 2.2 for comparison to the measured total collision frequency. In particular, the quasilinear theory of IAT that we have employed to derive an effective collision frequency relies on the assumption of a Maxwellian plasma. However, quasilinear energy exchange with the electron population causes a deviation from the thermalized plasma approximation and is characterized by a tail in the electron energy distribution function. This flatting of the distribution will reduce the rate of energy exchange with the waves, lowering the effective IAT. While we did not have an independent measure of the electron distribution function for this study, we note that if present this effect would suggest that our reported results are upper bounds for the non-classical collision frequency from the IAT. This tendency opposes our earlier expectations of an underestimated collision frequency due to drifting electrons, thus obscuring a clear trend in the systematic uncertainty. With that said, we still have found notable quantitative agreement in figure 6 between the electron collision frequency and the non-classical collision frequency.

In summary, we made the above assumptions to facilitate our analysis in light of limitations in experimental access and resources. While we have shown that these assumptions ultimately can impact our results, but our estimates of their influence indicate that they will not change our conclusions beyond the uncertainty bounds. We thus can still be confident in the time-resolved, physical correlation between the measured collision frequency and non-classical effects as well as our assessment of the applicability of proposed closure models that we later discuss in our companion paper [22]. The discussion above has underscored, however, that there is a need particularly for non-invasive, time-resolved plasma diagnostics such as Thomson scattering and laser-induced fluorescence [35, 38] to help resolve challenges related to probe perturbations and to resolve open questions related to the non-thermal nature of the distribution functions.

5.2. Physical implications for cathode modeling

Our results in figures 6 and 7 show experimentally, for the first time, the transient behavior of the electron collision frequency along the centerline of the discharge. We have shown that for the majority of the measured plume domain that this parameter can be described by the effective collision frequency due to the inherently kinetic effect of IAT wave growth. The region of quantitative disagreement near the cathode is thought to be the result of probe perturbations to the plasma, as we discussed earlier in section 5.1. This agreement between our measurements highlights the need for cathode models to not only capture the time-average effects of the wave-driven anomalous collision frequency but also the transient behavior. Indeed, the two numerical simulations of hollow cathodes performed to date that have shown large-scale instabilities qualitatively similar to the results we presented above have used time-resolved models for the anomalous collisions.

In practice, the approximations, or closures, these models employed for the collision frequency have differed and in turn have led to different physical conclusions about the underlying physics of the plume mode oscillation. For example, Mikellides *et al* [17] employed a saturated model for the IAT collision frequency and concluded that its relation to Ohmic heating of the electrons is essential to the development of the low-frequency plume mode oscillation. Our experimental measurements indeed show electron temperature fluctuations on the plume mode timescale, suggesting time-varying Ohmic heating may be a relevant driver for the wave. On the other hand,

Sary *et al* [16] employed a conservation equation for the IAT and a linear model for the growth rate to relate the IAT to a collision frequency. Their simulation shows that the periodic saturation of the IAT is the cause of the plume mode instability. In relation to our experimental measurements, we showed in figure 6 that the collision frequency, which depends strongly on the IAT wave energy density, has distinctly nonlinear structure. This finding suggests that periodic saturation of the IAT may also be a plausible explanation of the mode.

In summary, there are elements of these predictions that are consistent with our experiment. However, the qualitative comparison of our measurements to these existing theories does not provide definitive insight into the validity of either approach. This question ultimately only can be addressed by performing a quantitative comparison of these closure models to our experimental observations, which is the focus of the second part this work [22].

6. Conclusion

In conclusion, the goal of this work was to understand the evolution of the electron collision frequency over time in a hollow cathode plume exhibiting the large-scale plume mode instability. To this end, we used a phase averaging method to generate time-synced measurements of key plasma properties including density, temperature, potential, and the power spectrum of higher-frequency IAT fluctuations. These measurements showed that all of these these properties oscillate on the timescale (40 kHz) of the dominant, low-frequency plume mode oscillation. We used these parameters, combined with a quasi-1D Ohm's law, to calculate the electron collision frequency in space and time. By direct experimental comparison of these measurements to contributions from both classical and non-classical (i.e. wave-driven) electron transport, we showed that both the time-averaged and time-resolved electron collision frequency over most of the plume can be explained by IAT-driven contributions to the electron collision frequency. Although it has already been reported that the time-averaged IAT-driven effects dominate the cathode plume [18], this is the first time, to our knowledge, that this non-classical quantity has been shown to be the dominant driver of the transient electron collision frequency in the cathode plume. We evaluated this conclusion in light of potential sources of systematic uncertainty stemming from our experimental techniques but ultimately found that our conclusions are not impacted by these effects. Lastly, we discussed our results in the context of the hollow cathode models that have had the most success to date in modeling plume mode-like oscillations [16, 17]. In particular, both of these models have concluded that it is necessary to take into account the fact that non-classical resistance in the plume will be time-resolved. Our results support this conclusion, and indeed we found features in our measurements that were qualitatively consistent with the assumptions employed in both of these models about how the electron collision frequency should evolved in time. With that said, there is still a need to perform a quantitative evaluation to arrive at definitive insight on the validity of closure models for this effect and how these relate to the origins of the plume mode oscillation.

These outstanding questions are the subject of our follow-on investigation in part II.

ORCID iDs

Marcel P Georgin ⬛ https://orcid.org/0000-0003-3733-1682
Benjamin A Jorns ⬛ https://orcid.org/0000-0001-9296-2044

References

[1] Bernardus Franciscus Maria Pots 1979 Turbulence and transport in a magnetized argon plasma *PhD Thesis* Eindhoven Tech. Univ.
[2] Pots B F M, Coumans J J H and Schram D C 1981 *Phys. Fluid.* **24** 517–27
[3] Ngo M T, Schoenbach K H, Gerdin G A and Lee J H 1990 *IEEE Trans. Plasma Sci.* **18** 669–76
[4] Arbel D, Bar-Lev Z, Felsteiner J, Rosenberg A and Slutsker Y Z 1993 *Phys. Rev. Lett.* **71** 2919–22
[5] He S J, OuYang J T, Shang L and Feng H 2011 *IEEE Trans. Plasma Sci.* **39** 2514–5
[6] Dan M 2014 *J. Propul. Power* **30** 35–40
[7] Harrison W W and Magee C W 1974 *Anal. Chem.* **46** 461–4
[8] Muhl S and Pérez A 2015 *Thin Solid Films* **579** 174–98
[9] Goebel D M, Jameson K K, Katz I and Mikellides I G 2007 *Phys. Plasmas* **14** 103508 (1994-present)
[10] Mikellides I G, Katz I, Goebel D M, Jameson K K and Polk J E 2008 *J. Propul. Power* **24** 866–79
[11] Csiky G A 1969 Measurements of some properties of a discharge from a hollow cathode *Technical Note NASA*
[12] Philip C M 1971 *AIAA J.* **9** 2191–6
[13] Friedly V J and Wilbur P J 1992 *J. Propul. Power* **8** 635–43
[14] Georgin M P, Jorns B A and Gallimore A D 2019 *Phys. Plasmas* **26** 082308
[15] Sary G, Garrigues L and Boeuf J-P 2017 *Plasma Sources Sci. Technol.* **26** 055007
[16] Sary G, Garrigues L and Boeuf J-P 2017 *Plasma Sources Sci. Technol.* **26** 055008
[17] Mikellides I, Lopez Ortega A, Goebel D M and Becatti G 2020 *Plasma Sources Sci. Technol.* **29** 035003
[18] Jorns B A, Mikellides I G and Goebel D M 2014 *Phys. Rev. E* **90** 063106
[19] Jorns B A, Dodson C, Dan M, Goebel and Wirz R 2017 *Phys. Rev. E* **96** 023208
[20] Ortega A L, Jorns B A and Mikellides I G 2018 *J. Propul. Power* **34** 1026–38
[21] Sagdeev R Z and Galeev A A 1969 *Nonlinear Plasma Theory* (New York, NY: W.A. Benjamin)
[22] Georgin M P and Jorns B A 2020 *Plasma Sources Sci. Technol.* **29** 105011
[23] Mikellides I G, Katz I, Goebel D M and Jameson K K March 2007 *J. Appl. Phys.* **101** 063301
[24] Goebel D M and Katz I 2008 *Fundamentals of Electric Propulsion (Ion and Hall Thrusters)* vol 1 (New York: Wiley)

[25] Mikellides I, Katz I, Jameson K and Goebel D 2006 Driving processes in the orifice and near-plume regions of a hollow cathode 42nd *AIAA/ASME/SAE/ASEE Joint Propulsion Conf. & Exhibit*

[26] Katz I, Mikellides I and Goebel D 2004 Model of the plasma potential distribution in the plume of a hollow cathode *40th AIAA/ASME/SAE/ASEE Joint Propulsion Conf. and Exhibit* (Fort Lauderdale, Florida) (American Institute of Aeronautics and Astronautics)

[27] Katz I and Ioannis G M 2011 *J. Comput. Phys.* **230** 1454–64

[28] Huba J D 2016 *NRL Plasma Formulary* (Washington DC: The Office of Naval Research)

[29] Davidson R C and Krall N A 1977 *Nucl. Fusion* **17** 1313

[30] Goebel D M and Watkins R M 2010 *Rev. Sci. Instrum.* **81** 083504

[31] Sheehan J P and Hershkowitz N 2011 *Plasma Sources Sci. Technol.* **20** 063001

[32] Chen F F 2003 Langmuir probe diagnostics *IEEE-ICOPS Meeting* (Jeju, Korea) vol 2

[33] Jorns B A, Mikellides I G and Goebel D M 2014 Investigation of energetic ions in a 100-A hollow cathode *50th AIAA/ASME/SAE/ASEE Joint Propulsion Conf.* p 3826

[34] Dodson C, Jorns B A and Wirz R E 2019 *Plasma Sources Sci. Technol.* **28** 065009

[35] Dale E T and Jorns B A 2019 *Phys. Plasmas* **26** 013516

[36] Jorns B, Goebel D M and Hofer R R 2015 Plasma perturbations in high-speed probing of Hall thruster discharge chambers: quantification and mitigation *51st AIAA/SAE/ASEE Joint Propulsion Conf.*

[37] Grimaud L, Petin A, Vaudolon J and Mazouffre S 2016 *Rev. Sci. Instrum.* **87** 043506

[38] Vincent B, Tsikata S and Mazouffre S 2018 *Plasma Sources Sci. Technol.* **27** 055002

[39] Ito T and Cappelli M A 2009 *Appl. Phys. Lett.* **94** 211501

[40] Dodson C A, Perez-Grande D, Jorns B A, Goebel D M and Wirz R E 2018 *J. Propul. Power* **34** 1225–34

[41] Sheridan T E and Goree J 1994 *Phys. Rev.* E **50** 2991–6